ROYAL SOCIETY OF CHEMISTRY

Check for updates

Molecular optimization of incorporating pyran fused acceptor–donor–acceptor type acceptors enables over 15% efficiency in organic solar cells†

Simin Wu,[a] Lingxian Meng,[a] Zhe Zhang,[a] Mingpeng Li,[a] Yang Yang,[b] Jian Wang,[b] Hongbin Chen,[a] Changzun Jiang,[a] Xiangjian Wan, [ID][a] Chenxi Li,[a] Zhaoyang Yao*[a] and Yongsheng Chen [ID] *[a]

A series of acceptor–donor–acceptor type fused-ring non-fullerene acceptors, FOR-IN, FOR-1F and FOR-2F, were designed and synthesized, featuring the same pyran-composed backbone and different fluorine-substituted 1,1-dicyanomethylene-3-indanone terminals. The increased fluorine substitution in FOR-2F enhances its light harvesting capacity and electron mobility significantly, compared with the molecules FOR-IN and FOR-1F. With FOR-2F as the acceptor and the matching polymeric PM6 as the donor, their organic solar cells demonstrate a high performance of up to 15.18% power conversion efficiency. This is the highest performance reported to date for all pyran fused NFAs. In addition, the fluorine number- and location-induced variations of electronic property, charge transport, film morphology and photovoltaic property were investigated systematically.

Introduction

In the last few years, organic solar cells (OSCs) have gone through a rapid surge in development due to both the optimization of the active molecular structure and active layer morphology. Note that this is above their intrinsic merits of solution-processing, light weight, semi-transparency, flexibility and large-scale roll-to-roll production.[1–17] A typical OSC device usually employs an electron donor and acceptor blend as the light active layer, which plays a dominant role in the photovoltaic performance of OSCs.[18–31] Recently reported high-performance acceptor–donor–acceptor (A–D–A) type non-fullerene acceptors (NFAs) usually possess strong absorption in the near-infrared region and favorable molecular

[a] *State Key Laboratory and Institute of Elemento-Organic Chemistry, The Centre of Nanoscale Science and Technology and Key Laboratory of Functional Polymer Materials, Renewable Energy Conversion and Storage Center (RECAST), College of Chemistry, Nankai University, Tianjin 300071, China.*
E-mail: zyao@nankai.edu.cn, yschen99@nankia.edu.cn
[b] *The Institute of Seawater Desalination and Multipurpose Utilization, Ministry of Natural Resources (Tianjin), Tianjin 300192, China*
† Electronic supplementary information (ESI) available. See DOI: 10.1039/d1tc05779k

stacking, thereby generating a systematically enhanced photocurrent and voltage output.[32–40] However, so far, OSCs surpassing 18% power conversion efficiency (PCE) have been almost entirely based on Y6 and its analogues.[41–44] Besides the relatively ossified structures of the Y6 system, it is highly possible that lots of other distinctive A–D–A skeleton-based NFAs could achieve high-efficiency OSCs.[31,34,45] Therefore, it is very necessary to explore other types of NFAs with the aim of achieving state-of-the-art OSCs and beyond.

Pyran fused rings have been explored as distinctive blocks to construct a class of highly efficient NFAs.[11,37,46–58] Recently, our group developed an encouraging NFA, **FO-2F**,[45] featuring an easily synthesized pyran fused ring as the main building kernel. Note that **FO-2F**-based OSCs have afforded excellent PCEs, rendering them one of the most promising candidates for economically feasible OSC molecules. However, further improvement of their overall performance *via* structural modification still presents a great challenge. Based on our previous work, introducing alkyl chains at the β site of terminal thiophene has been proven as a feasible strategy to enlarge the V_{OC}[59] and enhance the device stability simultaneously by depressing the photo-decomposition of the NFAs.[60] In addition, halogen substitution usually acts as an effective way to tune their molecular energy levels and stacking models.[30,38,61–70] Specifically, fluorination on the end group of 2-(3-oxo-2,3-dihydro-1*H*-inden-1-ylidene)malononitrile (INCN)[71] can simultaneously down-shift the highest occupied molecular orbital (HOMO) and lowest unoccupied molecular orbital (LUMO) energy levels of NFAs without causing large steric hindrance.[72,73] Meanwhile, this could also improve the crystallinity and charge transport property of NFAs. Bearing these in mind, we designed three new acceptor molecules (Fig. 1) based on previously reported **FO-2F** by grafting an octyl group on terminal thiophene of the central donor part, which is expected to improve the voltage and stability of OSCs.[59,74]

Furthermore, different fluorine-substituted electron-withdrawing INCN units were end-capped with the central donor part above to afford three new NFAs (Fig. 1). These three NFAs possess stepwise lower LUMO energy levels from **FOR-IN** to **FOR-2F**, resulting in the strongest light absorption in the NIR region for **FOR-2F**. As a result,
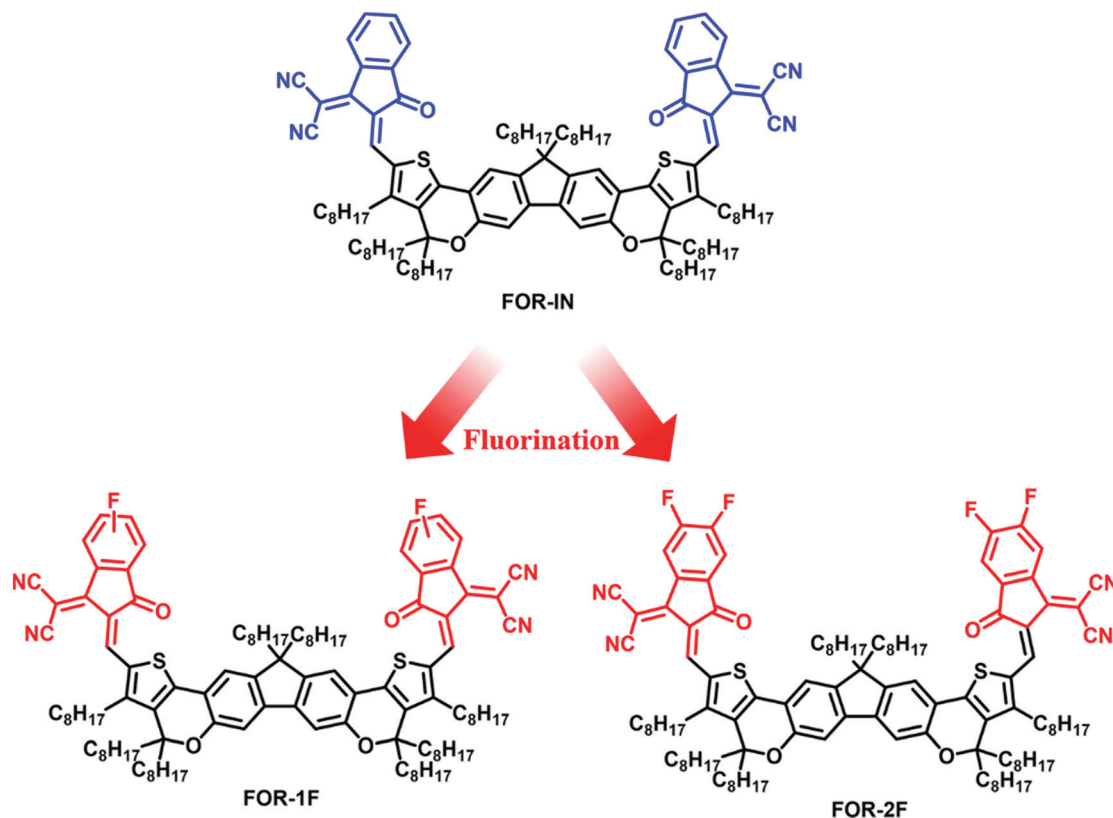
Fig. 1   Chemical structures of **FOR-IN**, **FOR-1F** and **FOR-2F**.

OSCs using **FOR-2F** and the well-known polymeric donor PM6 as the active layer achieved an excellent PCE of 15.18%, qualifying for the best performance reported to date for all pyran fused NFAs.

Synthesis and thermal properties

The synthetic routes for **FOR-IN**, **FOR-1F** and **FOR-2F** are shown in Scheme S1 (ESI†). The detailed procedures and characterization are summarized in the ESI.† The chemical structures of **FOR-IN**, **FOR-1F** and **FOR-2F** were fully characterized and confirmed by high-resolution mass spectrometry (HR-MS) and ^{1}H/^{13}C NMR. All the three molecules exhibit good solubility in commonly used solvents, such as dichloromethane, chloroform and chlorobenzene, in favour of the following solution-processing during the fabrication of OSCs. From the thermogravimetric analysis (TGA) curves in Fig. S2 (ESI†), all the three molecules were found to demonstrate great thermal stability, with **FOR-2F** having a slightly higher decomposition temperature (T_d) of 285 °C, compared with 280 °C for **FOR-IN** and 281 °C for **FOR-1F**.

Optical absorption and electrochemical properties

In order to evaluate the light harvesting ability of the three NFAs, we measured their ultraviolet-visible (UV-vis) absorption spectra in chloroform solutions and thin films (Fig. 2a and b), and the absorption spectra of the PM6:**FOR-IN**, PM6:**FOR-1F** and PM6:**FOR-2F** blend films are shown in Fig. S3 (ESI†). As expected, **FOR-2F** and **FOR-1F** exhibit a clear red-shifted absorption in chloroform solutions compared with that of **FOR-IN**, which should be ascribed to the fluorine-induced decrease of energy gaps. The maximum absorption peaks (λ_{max}) of **FOR-IN**, **FOR-1F** and **FOR-2F** bathochromically shift by 27, 36 and 52 nm from solution to solid states, respectively, suggesting the formation of stronger aggregates. More interestingly, the λ_{max} of the **FOR-2F** film exhibits further 21 nm red-shifting from 742 to 763 nm after thermal annealing, further driving its absorption onset (λ_{onset}) towards 810 nm. The further red-shifted light absorption can be expected to output a larger short-circuit current (J_{SC}) in OSCs. We further carried out cyclic voltammetry (CV) tests to investigate the experimental energy levels of **FOR-IN**, **FOR-1F** and **FOR-2F** (Fig. 2c). Based on the onset oxidation and reduction potentials, the HOMOs can be estimated as −5.70 eV for **FOR-IN**, −5.73 eV for **FOR-1F** and −5.76 eV for **FOR-2F**. Additionally, the LUMOs are calculated to be −3.67 eV for **FOR-IN**, −3.73 eV for **FOR-1F** and −3.76 eV for **FOR-2F**, thus resulting in stepwise decreased optical band gaps of **FOR-IN**, **FOR-1F** and **FOR-2F**, being 1.64 eV, 1.59 eV and 1.55 eV, respectively. The down-shifted HOMOs and LUMOs should be assigned to the substitution of fluorine atoms due to their large electronegativity.

Generally, the suitable alignment of energy levels and favourable decrease of energy gaps may result in an efficient OSC (Table 1).
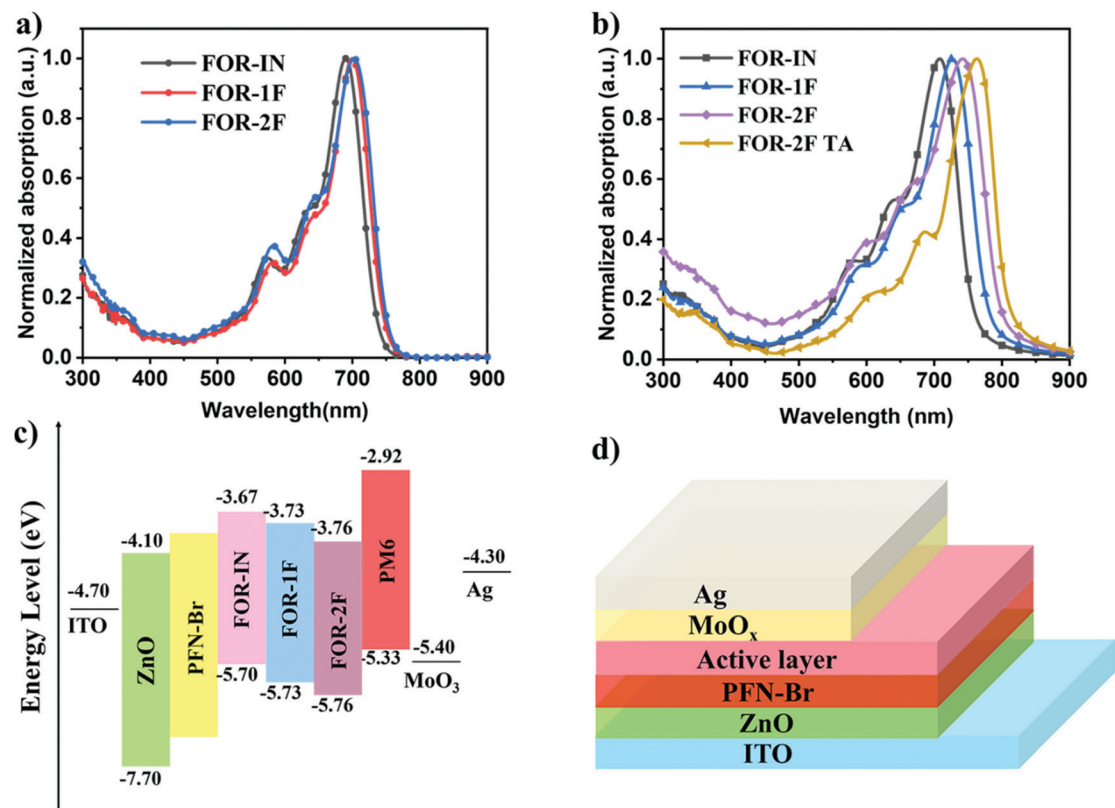
Fig. 2 (a) Normalized absorption spectra of **FOR-IN**, **FOR-1F** and **FOR-2F** in chloroform solution. (b) Normalized absorption spectra of as-cast films of **FOR-IN**, **FOR-1F**, **FOR-2F** and TA annealed film of **FOR-2F**. (c) Energy level diagram of each material used in OSCs. (d) Device structure of the OPVs studied here.

Table 1 Optical and electrochemical data of **FOR-IN**, **FOR-1F** and **FOR-2F**

Comp.	λ_{max}^{sol} [nm]	λ_{max}^{film} [nm]	HOMO [eV]	LUMO [eV]	λ_{onset} [nm]	$E_g^{Opt\ a}$ [eV]
FOR-IN	690	717	−5.70	−3.67	757	1.64
FOR-1F	700	736	−5.73	−3.73	780	1.59
FOR-2F	702	$742(763)^b$	−5.76	−3.76	$798(810)^b$	1.55(1.53)

^{a} Optical band gaps estimated from the absorption onset. ^{b} Absorption data with thermal annealing under 140 °C for 10 min.

Photovoltaic properties

To evaluate the photovoltaic properties of **FOR-IN**, **FOR-1F** and **FOR-2F**, we fabricated OSCs with an inverted structure of indium tin oxide (ITO)/ZnO/PFN-Br/active layer/MoO$_x$/Ag (Fig. 2d). Herein, PM6 was selected as the polymeric donor due to its matched energy levels and complementary absorption with the obtained NFAs. The optimal weight ratio (m%) of donors and NFAs was determined to be 1 : 1 and the detailed device parameters with various conditions are summarized in Tables S1–S10 in the ESI.† The corresponding optimal J–V characteristics are displayed in Fig. 3a and the best photovoltaic data of **FOR-IN**, **FOR-1F** and **FOR-2F** are summarized in Table 2. From **FOR-IN** to **FOR-2F**, stepwise decreased V_{OC} can be observed, being 1.071, 1.020 and 0.969 V, respectively, demonstrating their LUMO energy level dependence. It is worth noting that J_{SC} improves significantly from **FOR-IN** to **FOR-2F**, being

15.38, 18.65, and 21.25 mA cm^{-2}, respectively. The enhanced J_{SC} should be attributed to the obvious red-shifted absorption and more efficient charge separation and transport from **FOR-IN** to **FOR-2F**, as discussed below. Finally, with gradually improved fill factors, the OSCs employing **FOR-2F** as NFAs yield an impressive PCE of 15.18%, much better than that of the **FOR-IN**- and **FOR-1F**-based devices. Moreover, energy losses (E_{loss}) of the OSCs were calculated using the formula $E_{loss} = E_g - eV_{OC}$, giving rise to relatively small energy losses in the range of 0.56–0.57 eV. The observed result of enhanced performance of the OSCs due to the increasing fluorination of the end groups is consistent with the widely reported literatures.[63,65] External quantum efficiencies (EQEs) of the optimized devices are recorded in Fig. 3b, indicating an efficient photo-electron response of up to ∼810 nm for the **FOR-2F**-based OSCs. The clearly broadened photo-electron response and larger EQEs of **FOR-2F** with respect to the other two NFAs should be
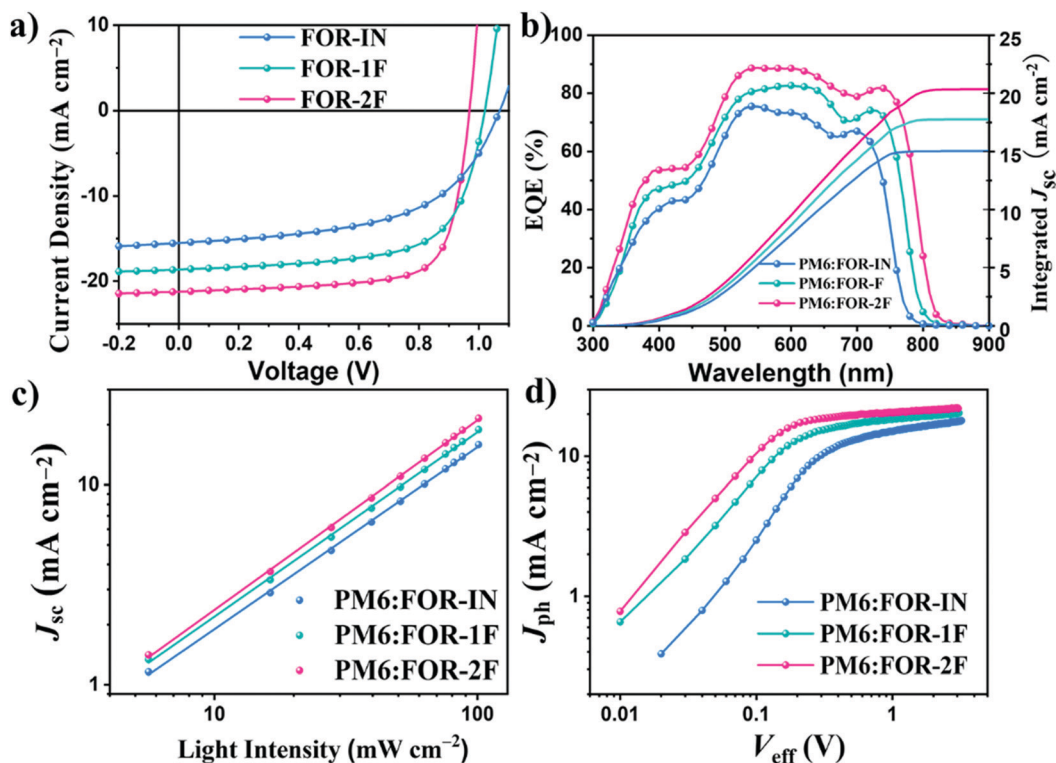
This journal is © The Royal Society of Chemistry 2022

J. Mater. Chem. C, 2022, **10**, 1977–1983 | **1979**

Fig. 3 (a) J–V characteristics and (b) EQE curves and integrated photocurrent from the EQE for the best devices. (c) J_{SC} *versus* light intensity of the optimized devices and (d) J_{ph} *versus* V_{eff} characteristics.

Table 2 Photovoltaic parameters of the **FOR-IN**-, **FOR-1F**- and **FOR-2F**-based optimized devices under the illumination of AM 1.5G (100 mW cm^{-2})

Device	V_{OC} [V]	J_{SC} [mA cm^{-2}]	FF [%]	PCE [%]	E_{loss} [eV]
FOR-IN	1.071	15.38	57.98	9.55(9.23)[a]	0.57
FOR-1F	1.020	18.65	66.21	12.59(12.29)[a]	0.57
FOR-2F	0.969	21.25	73.74	15.18(14.92)[a]	0.56

[a] The average PCEs provided in parentheses were obtained from 10 devices.

respectively ascribed to its red-shifted absorption and improved charge separation, as discussed below. Note that the integrated J_{SC} values for EQEs are in good agreement with the J_{SC} obtained from the J–V curves for the devices of all the three molecules.

In order to reveal the origin of EQE variation, we investigated the charge generation and charge recombination behaviour in the PM6:**FOR-IN**-, **FOR-1F**- and PM6:**FOR-2F**-based optimal devices. The photocurrent (J_{ph}) *versus* effective applied voltage (V_{eff}) curves were recorded and are presented in Fig. 3c. The charge dissociation probabilities can be calculated from J_{ph}/J_{sat} at the short-circuit condition, and are 87%, 90% and 93% for the **FOR-IN**- to **FOR-2F**-based devices, respectively. The enlarged charge dissociation probabilities suggest improved exciton dissociation efficiency for the **FOR-2F**-based OSC, in good accordance with the EQE spectra. Furthermore, we measured the light-intensity (P) dependence of J_{SC} to study the charge recombination properties (Fig. 3d). Based on the power-law equation $J_{SC} \propto P^{\alpha}$, the α values for the different OSCs of

FOR-IN, **FOR-1F** and **FOR-2F** are 0.911, 0.922 and 0.949, respectively. The close to unit α value indicates very few bimolecular recombinations in the devices, partially accounting for the high FF values of the OSCs.

The charge mobilities of the blend films of PM6:**FOR-IN**, PM6:**FOR-1F** and PM6:**FOR-2F** were estimated through the space-charge-limited current (SCLC) method (Fig. S5, ESI†). The PM6:**FOR-2F** photoactive layers exhibit a hole/electron mobility of $1.54 \times 10^{-4}/1.30 \times 10^{-4}$ cm^{-2} V^{-1} s^{-1}, which is higher than those of the **FOR-IN** ($6.71 \times 10^{-5}/5.55 \times 10^{-5}$ cm^{-2} V^{-1} s^{-1}) and **FOR-1F** ($8.99 \times 10^{-5}/7.12 \times 10^{-5}$ cm^{-2} V^{-1} s^{-1}) blend films. The higher hole and electron mobilities of PM6:**FOR-2F** should account for the increased FF of the resulting OSCs. Note that the charge mobilities increased with increased fluorination of the end groups, which could be attributed to the fluorine-induced strong molecular interactions.

Morphology characterization

As we all know, the morphologies of the active layers have a great influence on device performance; hence, we carried out transmission electron microscopy (TEM) and tapping-mode atomic force microscopy (AFM) to obtain morphology images of the active layers at the nanoscale, as shown in Fig. S7 (ESI†) and Fig. 4a–c.

In the TEM images, all the three blend films demonstrate finely dispersed phase separation with PM6. Furthermore, in
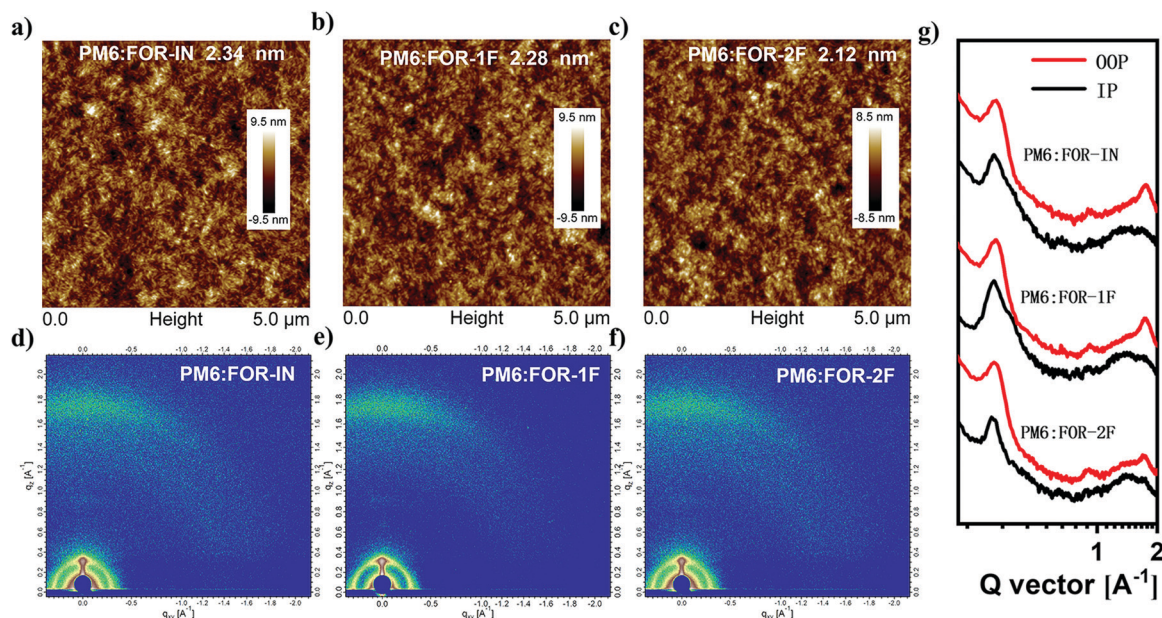
1980 | *J. Mater. Chem. C*, 2022, **10**, 1977–1983

This journal is © The Royal Society of Chemistry 2022

Fig. 4 AFM images of (a) PM6:**FOR-IN** blend film, (b) PM6:**FOR-1F** blend film and (c) PM6:**FOR-2F** blend film. GIWAXS pattern for (d) PM6:**FOR-IN** blend, (e) PM6:**FOR-1F** blend and (f) PM6:**FOR-2F** blend. (g) In-plane and out-of-plane line cuts of the corresponding GIWAXS patterns.

the AFM images, PM6:**FOR-2F** has a slightly smaller root-mean-square (RMS) surface roughness of 2.12 nm compared to 2.34 nm for PM6:**FOR-IN** and 2.28 nm for PM6:**FOR-1F**. Moreover, the line cuts of grazing-incidence wide-angle X-ray scattering (GIWAXS) patterns are shown in Fig. S6 (ESI†). The **FOR-2F** neat film shows strong π–π stacking diffraction peaks in both OOP and IP, suggesting a more ordered molecular packing compared with those of **FOR-IN** and **FOR-1F**. When blended with the PM6 donor (Fig. 4d–f), all the three blend films demonstrate a clear face-on orientation, indicated by the strong diffraction peaks at ∼1.73 Å^{-1} in the OOP direction. The π–π distance of the three blend films can be estimated as ∼3.65 Å, suggesting strong intermolecular action. As shown in Table S12 (ESI†), the crystal coherence lengths (CCL) in the (010) region for the **FOR-IN**-, **FOR-1F**- and **FOR-2F**-based blend films were calculated based on the Scherrer equation ($CCL = \dfrac{2\pi k}{fwhm}$), being 29.34, 33.31 and 41.23 Å, respectively. The intense π–π stacking and larger CCL of **FOR-2F** would facilitate its charge transport in the blend film, which is consistent with its higher electron mobility and improved photovoltaic performance compared to those of the other two NFAs.

Conclusion

Three new NFAs were designed and synthesized by capping fluorine-substituted end groups (INIC) with a pyran fused central donor. Among the three NFAs, the two fluorine substitution in **FOR-2F** drives the absorption of NFAs towards the near-infrared region and improves electron mobility greatly; hence, its OSC device demonstrates a highly enhanced J_{SC} of 21.25 mA cm^{-2}, FF of ∼74%, and V_{OC} of 969 mV, affording an excellent PCE of 15.18%. This renders it as the highest value reported to date in pyran fused

NFAs. These results demonstrate that other A–D–A type molecular systems, through symmetric optimization, could also offer desirable organic photovoltaic molecules, providing another potentially new molecular system to further improve organic photovoltaic performance.

Conflicts of interest

The authors declare no conflict of interest.

Acknowledgements

Notes and references

1 L. Zhu, M. Zhang, W. Zhong, S. Leng, G. Zhou, Y. Zou, X. Su, H. Ding, P. Gu, F. Liu and Y. Zhang, *Energy Environ. Sci.*, 2021, **14**, 4341–4357.

2 Z. G. Zhang and Y. Li, *Angew. Chem., Int. Ed.*, 2021, **60**, 4422–4433.

3 X. Zhang, L. Qin, J. Yu, Y. Li, Y. Wei, X. Liu, X. Lu, F. Gao and H. Huang, *Angew. Chem., Int. Ed.*, 2021, **60**, 12475–12481.

4 J. Zhang, Y. Xiang and S. Zheng, *New J. Chem.*, 2021, **45**, 12247–12259.

5 H. Feng, Y.-Q.-Q. Yi, X. Ke, Y. Zhang, X. Wan, C. Li and Y. Chen, *Sol. RRL*, 2018, **2**, 1800053.

6 Y. Huo, X.-T. Gong, T.-K. Lau, T. Xiao, C. Yan, X. Lu, G. Lu, X. Zhan and H.-L. Zhang, *Chem. Mater.*, 2018, **30**, 8661–8668.

This journal is © The Royal Society of Chemistry 2022

J. Mater. Chem. C, 2022, **10**, 1977–1983 | **1981**

7   Y. Xie, W. Huang, Q. Liang, J. Zhu, Z. Cong, F. Lin, S. Yi, G. Luo, T. Yang, S. Liu, Z. He, Y. Liang, X. Zhan, C. Gao, H. Wu and Y. Cao, *ACS Energy Lett.*, 2018, **4**, 8–16.

8   Y. T. Hsiao, C. H. Li, S. L. Chang, S. Heo, K. Tajima, Y. J. Cheng and C. S. Hsu, *ACS Appl. Mater. Interfaces*, 2017, **9**, 42035–42042.

9   Y. J. Cheng, C. H. Chen, T. Y. Lin and C. S. Hsu, *Chem. – Asian J.*, 2012, **7**, 818–825.

10 T.-W. Chen, K.-L. Peng, Y.-W. Lin, Y.-J. Su, K.-J. Ma, L. Hong, C.-C. Chang, J. Hou and C.-S. Hsu, *J. Mater. Chem. A*, 2020, **8**, 1131–1137.

11 L. Meng, Y. Zhang, X. Wan, C. Li, X. Zhang, Y. Wang, X. Ke, Z. Xiao, L. Ding, R. Xia, H.-L. Yip, Y. Cao and Y. Chen, *Science*, 2018, **361**, 1094–1098.

12 R. Ma, T. Liu, Z. Luo, Q. Guo, Y. Xiao, Y. Chen, X. Li, S. Luo, X. Lu, M. Zhang, Y. Li and H. Yan, *Sci. China: Chem.*, 2020, **63**, 325–330.

13 Q. Wu, D. Deng, J. Zhang, W. Zou, Y. Yang, Z. Wang, H. Li, R. Zhou, K. Lu and Z. Wei, *Sci. China: Chem.*, 2019, **62**, 837–844.

14 M. Chen, Z. Zhang, W. Li, J. Cai, J. Yu, E. L. K. Spooner, R. C. Kilbride, D. Li, B. Du, R. S. Gurney, D. Liu, W. Tang, D. G. Lidzey and T. Wang, *Sci. China: Chem.*, 2019, **62**, 1221–1229.

15 B. Fan, L. Ying, F. Huang and Y. Cao, *J. Mater. Chem. C*, 2016, **4**, 8052–8060.

16 C. Li, Y. Xie, B. Fan, G. Han, Y. Yi and Y. Sun, *J. Mater. Chem. C*, 2018, **6**, 4873–4877.

17 Y. Zuo, W. Ni, Q. Zhang, M. Li, B. Kan, X. Wan and Y. Chen, *J. Mater. Chem. C*, 2014, **2**, 7247.

18 T. Jia, J. Zhang, W. Zhong, Y. Liang, K. Zhang, S. Dong, L. Ying, F. Liu, X. Wang, F. Huang and Y. Cao, *Nano Energy*, 2020, **72**, 104718.

19 X. Chen, B. Kan, Y. Kan, M. Zhang, S. B. Jo, K. Gao, F. Lin, F. Liu, X. Peng, Y. Cao and A. K. Y. Jen, *Adv. Funct. Mater.*, 2020, **30**, 1909535.

20 Q. Zhang, Y. Sun, X. Chen, Z. Lin, X. Ke, X. Wang, T. He, S. Yin, Y. Chen and H. Qiu, *J. Mater. Chem. C*, 2019, **7**, 5381–5384.

21 Y.-Q.-Q. Yi, H. Feng, N. Zheng, X. Ke, B. Kan, M. Chang, Z. Xie, X. Wan, C. Li and Y. Chen, *Chem. Mater.*, 2019, **31**, 904–911.

22 Y. Lin, J. Wang, Z. G. Zhang, H. Bai, Y. Li, D. Zhu and X. Zhan, *Adv. Mater.*, 2015, **27**, 1170–1174.

23 A. Tang, W. Song, B. Xiao, J. Guo, J. Min, Z. Ge, J. Zhang, Z. Wei and E. Zhou, *Chem. Mater.*, 2019, **31**, 3941–3947.

24 H. Lai, H. Chen, J. Zhou, J. Qu, M. Wang, W. Xie, Z. Xie and F. He, *J. Phys. Chem. Lett.*, 2019, **10**, 4737–4743.

25 D. Liu, B. Yang, B. Jang, B. Xu, S. Zhang, C. He, H. Y. Woo and J. Hou, *Energy Environ. Sci.*, 2017, **10**, 546–551.

26 S. Li, L. Ye, W. Zhao, X. Liu, J. Zhu, H. Ade and J. Hou, *Adv. Mater.*, 2017, **29**, 1704051.

27 W. Gao, M. Zhang, T. Liu, R. Ming, Q. An, K. Wu, D. Xie, Z. Luo, C. Zhong, F. Liu, F. Zhang, H. Yan and C. Yang, *Adv. Mater.*, 2018, **30**, 1800052.

28 X. Li, H. Huang, H. Bin, Z. Peng, C. Zhu, L. Xue, Z.-G. Zhang, Z. Zhang, H. Ade and Y. Li, *Chem. Mater.*, 2017, **29**, 10130–10138.

29 J. Liang, P. Yin, T. Zheng, G. Wang, X. Zeng, C. Cui and P. Shen, *J. Mater. Chem. C*, 2019, **7**, 10028–10038.

30 Y. Cui, C. Yang, H. Yao, J. Zhu, Y. Wang, G. Jia, F. Gao and J. Hou, *Adv. Mater.*, 2017, **29**, 1703080.

31 X. Wan, C. Li, M. Zhang and Y. Chen, *Chem. Soc. Rev.*, 2020, **49**, 2828–2842.

32 Y. Liu and Y. Chen, *Adv. Mater.*, 2020, **32**, 1805843.

33 J. Yuan, Y. Zhang, L. Zhou, G. Zhang, H.-L. Yip, T.-K. Lau, X. Lu, C. Zhu, H. Peng, P. A. Johnson, M. Leclerc, Y. Cao, J. Ulanski, Y. Li and Y. Zou, *Joule*, 2019, **3**, 1140–1151.

34 Y. Ma, M. Zhang, S. Wan, P. Yin, P. Wang, D. Cai, F. Liu and Q. Zheng, *Joule*, 2020, **5**, 197–209.

35 Y. Cui, H. Yao, J. Zhang, T. Zhang, Y. Wang, L. Hong, K. Xian, B. Xu, S. Zhang, J. Peng, Z. Wei, F. Gao and J. Hou, *Nat. Commun.*, 2019, **10**, 2515.

36 B. Fan, D. Zhang, M. Li, W. Zhong, Z. Zeng, L. Ying, F. Huang and Y. Cao, *Sci. China: Chem.*, 2019, **62**, 746–752.

37 Y. Zhou, M. Li, J. Song, Y. Liu, J. Zhang, L. Yang, Z. Zhang, Z. Bo and H. Wang, *Nano Energy*, 2018, **45**, 10–20.

38 B. Kan, H. Feng, H. Yao, M. Chang, X. Wan, C. Li, J. Hou and Y. Chen, *Sci. China: Chem.*, 2018, **61**, 1307–1313.

39 R. Hou, M. Li, J. Wang, Z. Bi, S. Feng, X. Xu, W. Ma and Z. Bo, *J. Mater. Chem. C*, 2019, **7**, 3335–3341.

40 Z. H. Zhang, X. Liu, J. S. Yu, H. T. Wang, M. Zhang, L. A. Yang, R. Y. Geng, J. R. Cao, F. A. Du, F. Liu and W. H. Tang, *J. Mater. Chem. C*, 2019, **7**, 13279–13286.

41 M. Zhang, L. Zhu, T. Hao, G. Zhou, C. Qiu, Z. Zhao, N. Hartmann, B. Xiao, Y. Zou, W. Feng, H. Zhu, M. Zhang, Y. Zhang, Y. Li, T. P. Russell and F. Liu, *Adv. Mater.*, 2021, **33**, 2007177.

42 M. Zhang, L. Zhu, G. Zhou, T. Hao, C. Qiu, Z. Zhao, Q. Hu, B. W. Larson, H. Zhu, Z. Ma, Z. Tang, W. Feng, Y. Zhang, T. P. Russell and F. Liu, *Nat. Commun.*, 2021, **12**, 309.

43 Y. Li, Y. Cai, Y. Xie, J. Song, H. Wu, Z. Tang, J. Zhang, F. Huang and Y. Sun, *Energy Environ. Sci.*, 2021, **14**, 5009–5016.

44 Y. Cui, Y. Xu, H. Yao, P. Bi, L. Hong, J. Zhang, Y. Zu, T. Zhang, J. Qin, J. Ren, Z. Chen, C. He, X. Hao, Z. Wei and J. Hou, *Adv. Mater.*, 2021, **33**, 2102420.

45 X. Ke, L. Meng, X. Wan, M. Li, Y. Sun, Z. Guo, S. Wu, H. Zhang, C. Li and Y. Chen, *J. Mater. Chem. A*, 2020, **8**, 9726–9732.

46 A. Efrem, K. Wang and M. Wang, *Dyes Pigm.*, 2017, **145**, 331–338.

47 W. Li, Z. Xiao, J. Cai, J. A. Smith, E. L. K. Spooner, R. C. Kilbride, O. S. Game, X. Meng, D. Li, H. Zhang, M. Chen, R. S. Gurney, D. Liu, R. A. L. Jones, D. G. Lidzey, L. Ding and T. Wang, *Nano Energy*, 2019, **61**, 318–326.

48 X. Ma, Z. Xiao, Q. An, M. Zhang, Z. Hu, J. Wang, L. Ding and F. Zhang, *J. Mater. Chem. A*, 2018, **6**, 21485–21492.

49 T. Li, H. Zhang, Z. Xiao, J. J. Rech, H. Niu, W. You and L. Ding, *Mater. Chem. Front.*, 2018, **2**, 700–703.

50 Z. Xiao, F. Liu, X. Geng, J. Zhang, S. Wang, Y. Xie, Z. Li, H. Yang, Y. Yuan and L. Ding, *Sci. Bull.*, 2017, **62**, 1331–1336.

51 M. Li, Y. Guo, Y. Zhou, J. Zhang, L. Yang, L. Zhang, J. Song, Z. Bo and H. Wang, *ACS Appl. Mater. Interfaces*, 2018, **10**, 13931–13940.

1982 | *J. Mater. Chem. C*, 2022, **10**, 1977–1983

This journal is © The Royal Society of Chemistry 2022

52 Z. Xiao, S. Yang, Z. Yang, J. Yang, H. L. Yip, F. Zhang, F. He, T. Wang, J. Wang, Y. Yuan, H. Yang, M. Wang and L. Ding, *Adv. Mater.*, 2019, **31**, 1804790.

53 C. Xia, H. Wu, Q. Yue, S. Chen, L. Shui, H. Fan and X. Zhu, *J. Mater. Chem. C*, 2019, **7**, 15344–15349.

54 H. Wu, H. Fan, S. Xu, L. Ye, Y. Guo, Y. Yi, H. Ade and X. Zhu, *Small*, 2019, **15**, 1804271.

55 Z. Liu, X. Zhang, P. Ren, Y. Wu, D. Zeng, X. Duan, X. Gao and P. Cai, *Sol. Energy*, 2019, **183**, 463–468.

56 L. Yang, M. Li, J. Song, Y. Zhou, Z. Bo and H. Wang, *Adv. Funct. Mater.*, 2018, **28**, 1705927.

57 M. Li, Y. Zhou, L. Yang, S. Shen, Y. Liu, Y. Chen, J. Song and Z. Bo, *J. Mater. Chem. A*, 2020, **8**, 22416–22422.

58 M. Li, Y. Liu, Y. Zhou, L. Yang, S. Shen, J. Song and Z. Bo, *ACS Appl. Mater. Interfaces*, 2020, **12**, 4887–4894.

59 H. H. Gao, Y. Sun, Y. Cai, X. Wan, L. Meng, X. Ke, S. Li, Y. Zhang, R. Xia, N. Zheng, Z. Xie, C. Li, M. Zhang, H. L. Yip, Y. Cao and Y. Chen, *Adv. Energy Mater.*, 2019, **9**, 1901024.

60 Z.-X. Liu, Z.-P. Yu, Z. Shen, C. He, T.-K. Lau, Z. Chen, H. Zhu, X. Lu, Z. Xie, H. Chen and C.-Z. Li, *Nat. Commun.*, 2021, **12**, 3049.

61 T. Zhang, G. Zeng, F. Ye, X. Zhao and X. Yang, *Adv. Energy Mater.*, 2018, **8**, 1801387.

62 J. Sun, X. Ma, Z. Zhang, J. Yu, J. Zhou, X. Yin, L. Yang, R. Geng, R. Zhu, F. Zhang and W. Tang, *Adv. Mater.*, 2018, **30**, 1707150.

63 W. Zhao, S. Li, H. Yao, S. Zhang, Y. Zhang, B. Yang and J. Hou, *J. Am. Chem. Soc.*, 2017, **139**, 7148–7151.

64 F. Yang, C. Li, W. Lai, A. Zhang, H. Huang and W. Li, *Mater. Chem. Front.*, 2017, **1**, 1389–1395.

65 S. Dai, F. Zhao, Q. Zhang, T. K. Lau, T. Li, K. Liu, Q. Ling, C. Wang, X. Lu, W. You and X. Zhan, *J. Am. Chem. Soc.*, 2017, **139**, 1336–1343.

66 D. Deng, Y. Zhang, J. Zhang, Z. Wang, L. Zhu, J. Fang, B. Xia, Z. Wang, K. Lu, W. Ma and Z. Wei, *Nat. Commun.*, 2016, **7**, 13740.

67 J. Zhang, Y. Li, H. Hu, G. Zhang, H. Ade and H. Yan, *Chem. Mater.*, 2019, **31**, 6672–6676.

68 Y. Li, J. D. Lin, X. Che, Y. Qu, F. Liu, L. S. Liao and S. R. Forrest, *J. Am. Chem. Soc.*, 2017, **139**, 17114–17119.

69 Y. Sun, H.-H. Gao, Y.-Q.-Q. Yi, X. Wan, H. Feng, X. Ke, Y. Zhang, J. Yan, C. Li and Y. Chen, *Sci. China Mater.*, 2019, **62**, 1210–1217.

70 H.-H. Gao, Y. Sun, X. Wan, B. Kan, X. Ke, H. Zhang, C. Li and Y. Chen, *Sci. China Mater.*, 2017, **60**, 819–828.

71 M. Li, Y. Liu, W. Ni, F. Liu, H. Feng, Y. Zhang, T. Liu, H. Zhang, X. Wan, B. Kan, Q. Zhang, T. P. Russell and Y. Chen, *J. Mater. Chem. A*, 2016, **4**, 10409–10413.

72 K. Reichenbacher, H. I. Suss and J. Hulliger, *Chem. Soc. Rev.*, 2005, **34**, 22–30.

73 L. Lu and L. Yu, *Adv. Mater.*, 2014, **26**, 4413–4430.

74 X. Zhang, C. Li, L. Qin, H. Chen, J. Yu, Y. Wei, X. Liu, J. Zhang, Z. Wei, F. Gao, Q. Peng and H. Huang, *Angew. Chem., Int. Ed.*, 2021, **60**, 17720–17725.